Morphometric variance, evolutionary constraints and their change through time in Late Devonian Palmatolepis conodonts

Sabrina Renaud, Catherine Girard, Anne-béatrice Dufour

Morphometric variance, evolutionary constraints and their change through time in Late Devonian *Palmatolepis* conodonts

Sabrina RENAUD [1], Catherine GIRARD [2], Anne-Béatrice DUFOUR [1]

[1] Laboratoire de Biométrie et Biologie Evolutive, UMR 5558, CNRS, Université Claude Bernard Lyon 1, Université de Lyon, 69622, Villeurbanne, France. * Corresponding author. Sabrina.Renaud@univ-lyon1.fr

[2] Institut des Sciences de l'Evolution de Montpellier (ISEM), Université de Montpellier, CNRS, EPHE, IRD, Montpellier, France

Published version:

Evolution, 75(11): 2911-2929.

doi: https://doi.org/10.1111/evo.14330

Abstract

Phenotypic variation is the raw material of evolution. Standing variation can facilitate response to selection along "lines of least evolutionary resistance", but selection itself might alter the structure of the variance. Shape was quantified using 2D geometric morphometrics in *Palmatolepis* conodonts through the Late Devonian period. Patterns of variance were characterized along the record by the variance-covariance matrix (P-matrix) and its first axis (Pmax). The Late Frasnian was marked by environmental oscillations culminating with the Frasnian/Famennian mass extinction. A shape response was associated with these fluctuations, together with a deflection of the Pmax and the P-matrix. Thereafter, along the Famennian, *Palmatolepis* mean shape shifted from broad elements with a large platform to slender elements devoid of platform. This shift in shape was associated with a reorientation of Pmax and the P-matrix, due to profound changes in the functioning of the elements selecting for new types of variants. Both cases provide empirical evidences that moving adaptive optimum can reorient phenotypic variation, boosting response to environmental changes. On such time scales, the question seems thus not to be whether the P-matrix is stable, but how it is varying in response to changes in selection regimes and shifts in adaptive optimum.

Keywords

Geometric morphometrics, outline analysis, Pmax, P-matrix, DISTATIS, Famennian

ORCID references

Sabrina RENAUD : 0000-0002-8730-3113

Catherine GIRARD : 0000-0003-3123-8276

Anne-Béatrice DUFOUR : 0000-0002-9339-4293

Introduction

Phenotypic variation is the raw material of evolution. The potential for adaptive responses is determined by the extent of variation available to the screening of selection, and the structure of the genetic covariations that represent constraints due to the interrelationships between traits. Response to selection can be impeded if the covariation between traits is unfavorable (Arnold et al. 2001; Steppan et al. 2002) whereas it can be deflected towards the traits combinations that have the most variation, constituting line of least resistance to evolution (Schluter 1996). This has been formalized based on the quantification of the variance-covariance genetic matrix (G matrix) and its main direction (Gmax) (Steppan et al. 2002; Bégin and Roff 2003; McGuigan et al. 2005). However, morphology is the only information to retrace the evolutionary history of ancient fossils, degradation preventing the extraction of genetic information. In such case, the G-matrix cannot be estimated, but the matrix of phenotypic variance-covariance, or P-matrix, could be used instead. G represents the portion of P that is heritable (Polly 2004). Heritability of morphological characters seems to be intermediate to high (Cheverud 1988), for instance reaching >60% for the shape of feeding structures in mice (Pallares et al. 2014; Pallares et al. 2017). This makes P a good surrogate for G in the fossil record (Renaud et al. 2006; Hunt 2007).

Estimating P-matrices in the fossil record could allow to test predictions regarding its stability vs. temporal changes. The G/P-matrix can be altered by selection, with variation being enhanced in the direction of an adaptive peak (Eroukhmanoff 2009) or along a moving adaptive optimum (Jones et al. 2012). In this case, G/P could “store” ancient environmental pressures, strengthening or weakening its constraining effect on future selection pressures (Eroukhmanoff 2009; McGlothlin et al. 2018). Extreme environmental changes are thus expected not only to exert strong selective pressure on shape itself, but also to affect P, whereas response to moderate environmental changes are more likely to surf on the line of least resistance characterized by the directions of main variance.

The Late Devonian (382 to 359 Ma) offers opportunities to assess the impact of environmental changes of various intensity and duration on organisms. The Frasnian / Famennian boundary (F/F), 371 Ma ago, was marked by one of the major mass extinction in Earth’s history (McGhee 1996). The mass extinction was the culmination of a perturbation materialized by anoxic deposits in many marine environments (the Upper Kellwasser Event, or UKE); it was associated with a pronounced temperature decrease and sea-level fall (Girard and Renaud 2007). This event was preceded, *ca*. 2 myrs before, by another event of similar nature (the Lower Kellwasser Event, or LKE) but of lesser impact on the biosphere (Joachimski and Buggisch 2002; Girard and Renaud 2007). A temperature decrease associated with a sea-level shallowing occurred towards the end of the LKE. The interval

between the two events was then marked by a progressive temperature increase and sea-level rise (Girard and Renaud 2007). Following the F/F crisis, temperatures were stable for a while (*ca.* 2 myrs) and thereafter launched a progressive decrease towards values much colder than the pre-LKE temperatures (Joachimski et al. 2009). This period thus offers the opportunity to investigate the response of organisms to environmental changes of different paces and amplitudes.

Conodonts are long extinct fossils without modern equivalent. These early vertebrates were small eel-like predators and an important part of the nektonic fauna increasing in richness through the Paleozoic period (Purnell 1995). They had a well-developed feeding apparatus composed of several tooth-like elements of complex shapes. Anterior elements formed a trapping structure, whereas posterior elements processed food items (Aldridge et al. 1987; Purnell and Donoghue 1997). Platform elements P1 (Supp. Fig. 1), located at the rear of the conodont mouth, functioned with an occlusion between right and left elements, sometimes leading to a pronounced asymmetry (Donoghue and Purnell 1999; Martínez-Pérez et al. 2016; Renaud et al. 2021). Conodont elements grew by the incremental addition of lamellae. Anisometric growth, with zones characterized by thicker lamellae, caused changes in the shape of many elements (Girard and Renaud 2008; Chen et al. 2016). Being composed of apatite, conodont elements are extremely resistant and are abundant in the fossil record. P1 elements, in particular, displayed a robust shape and a rapid morphological evolution that made them highly used stratigraphic markers, and the focus of many morphometric studies, e.g. (Klapper and Foster 1986; Renaud and Girard 1999; Jones et al. 2009; Chen et al. 2016; Hogancamp et al. 2016).

Palmatolepis is the emblematic genus of the Late Devonian (Klapper 1989; Ziegler and Sandberg 1990). Its P1 elements were characterized by a reduced bilateral asymmetry (Renaud and Girard 1999) and allometric growth (Girard et al. 2007). Shape changes were documented during the interval preceding the F/F crisis, and appeared correlated with temperature (Balter et al. 2008). A large-scale morphological trend was further documented along the Famennian (Girard and Renaud 2012). *Palmatolepis* thus constitutes a good model to quantify shape and shape variation during the Late Devonian period, and assess how the P-matrix was affected by environmental changes of various magnitude and pace.

Using a geometric morphometric approach based on an outline analysis of the P1 element, *Palmatolepis* shape was therefore quantified along a record covering the Latest Frasnian and the Famennian. Along this record, the direction of allometric variation, the P-matrix and its first direction, Pmax, as well as evolutionary trajectories characterizing temporal evolution and diversification within *Palmatolepis*, were quantified to test the following main hypotheses. (1) Given

the magnitude of the environmental changes along the record, *Palmatolepis* likely faced moving adaptive optima; this could have selected for new types of variants, thus reorienting Pmax and the P-matrix. (2) Allometry should constitute an important component of the phenotypic variation, and thus be correlated with Pmax. (3) The stability of Pmax and the P-matrix, and their role in channelling evolution, could have been modulated by the magnitude and pace of the environmental fluctuations. During periods of relatively stable environmental conditions, Pmax and the P-matrix should be conserved; shape should evolve following the line of least resistance Pmax, and possibly the allometric direction. In contrast, during periods of intense perturbations, flexibility may override constraints (Beldade et al. 2002), and shape evolution may deviate from Pmax. Pmax and the P-matrix could be deflected due to moving adaptive optimum (Eroukhmanoff 2009).

Material and Methods

Fossil material for morphometric analyses

The Col des Tribes section (CT, Montagne Noire, France) exposes an almost continuous record from Late Frasnian to Late Famennian deposits (-378 to -360 Ma) (Girard et al. 2014). Conodont elements were picked in seven Frasnian and twelve Famennian levels, designed according to the bed numbering in the outcrop (Girard et al. 2014). A few grams of rocks were enough to deliver hundreds of elements (Girard et al. 2014). To minimize time averaging, efforts were done to sample the piece of rock within few centimeters at basis of each stratigraphic level. Oxygen isotopes were measured on the apatite of conodonts picked in the same levels (Girard et al. 2020). Age was estimated for each level using a biostratigraphic analysis (Girard et al. 2014) based on the zonations defined for the Frasnian (Klapper and Kirchgasser 2016) and the Famennian (Spalletta et al. 2017). Absolute ages were estimated according to the current datation framework (Becker et al. 2020). Among the Frasnian levels, CT_06 is situated just after the LKE whereas CT_23 is located just before the F/F boundary (Fig. 1).

Numerous stratigraphic species and even subspecies have been described within *Palmatolepis*, as a way to describe the extensive morphological variation. Rather than being distinct evolutionary units, however, they often correspond to end-members of continuous morphological variation (Scott and Collinson 1959; Girard and Renaud 2011). In contrast, subgenera correspond to relatively well identified ranges of the morphospace (Girard and Renaud 2012). Hence, considering the subgenus as unit seems a relevant approach to assess temporal changes in mean shape and morphological variance (Girard et al. 2004; Girard and Renaud 2011). Furthermore, reliably assessing shape variance requires good sample size, ideally above 30 specimens per sample (Cardini and Elton 2007). Hence,

the sampling of this study was targeted at four well-represented subgenera presented thereafter (Table 1; Fig. 1; descriptive terminology and the orientation of the element: Supp. Fig. 1).

(1) *Manticolepis* is characteristic of the Late Frasnian. Its P1 elements display a large, wide platform with a well-developed outer lobe (Müller 1956). The carina is more or less sigmoidal. There is broad consensus as to the taxonomic limits of this subgenus since its inception (Helms 1963; van den Boogaard and Kuhry 1979).

(2) *Panderolepis* P1 elements are characterized by the narrowness of the platform, with an almost absent lateral lobe. In the initial description of the subgenus (Helms 1963), two species were included: *glabra* and *tenuipunctata*, with the hypothesis that *Pa. (Panderolepis) glabra* evolved from *tenuipunctata* by the loss of the outer lobe and the development of a parapet at the anterior, inner part (also called ventral, caudal part) of the platform. This was later challenged by authors proposing that *tenuipunctata* was the only Frasnian survivor of the *Manticolepis* subgenus (van den Boogaard and Kuhry 1979). The initial delineation of the subgenus was retained, but the early sample from the Col des Tribes (PAN_35) is composed of *tenuipunctata* and late samples (PAN_50 and later) are composed of *glabra*. The sample PAN_37 is composed of a mix of both species (12 *glabra* and 30 *tenuipunctata*).

(3) *Deflectolepis* has been initially described based on the morphology of the P1 element (Müller 1956). They have a very narrow platform, reduced to margins paralleling the carina. Two species are documented. *Palmatolepis (Deflectolepis) gracilis* has a smooth surface. *Palmatolepis (Deflectolepis) minuta* is characterized by a straight carina and a platform that is slightly developed, and which sometimes displays a small lateral lobe. The homogeneity of this subgenus has been challenged based on few multi-element reconstructions, suggesting that the two species differed by their P2 element (van den Boogaard and Kuhry 1979). As this study focuses on P1 elements, the delineation of the subgenus based on this element was retained, but its homogeneity was questioned. The early samples from the Col des Tribes (DEF_41 and DEF_42) are composed of *minuta* whereas the later samples (DEF_45 and later) are almost exclusively composed of *gracilis*, to the exception of two *minuta* specimens in the level DEF_59.

(4) *"rhomboidea"* is not strictly speaking a subgenus, but it was constantly set apart from other subgenera because of its very characteristic platform of rhombohedral shape (Müller 1956; Helms 1963). The outer lobe is usually reduced. The blade-carina line is usually sigmoidal.

The Operational Taxonomic Units (OTUs) were groups corresponding to the subgenus x stratigraphic level. Each OTU included all entire P1 conodont elements of the concerned subgenus picked in the given level, except in PAN_51 in which only right elements were considered, due to an exceptional

abundance in this level. The resulting sampling encompassed 22 OTUs, for a total of 1435 P1 conodont elements (Table 1). Note that phylogenetic relationships between subgenera have been proposed (Müller 1956; Helms and Ziegler 1981) but they remain largely hypothetical. This precluded the possibility to perform phylogenetically-controlled morphometric analyses.

Methods of morphometric and multivariate analyses

Outline extraction and quantification. – Pictures of the conodont elements were taken, the element lying flat on its platform, the blade upward (Fig. 1). Left elements were mirrored and measured as right elements; both right and left elements were analyzed together (Renaud and Girard 1999). The outline of the platform was quantified using 64 equally-spaced points extracted using the image analysis software Optimas, the starting point being positioned at the tip of the carina. Radii (i.e. distance of each point to the center of gravity of the points) were calculated from these coordinates. The empirical function of the radius as a function of the cumulated distance along the outline was decomposed into a sum of trigonometric functions of decreasing wavelengths (the harmonics). Each harmonic is weighted by two Fourier coefficients (FCs) that constitute the shape variables. This method, implemented in the R package Momocs (Bonhomme et al. 2014), has been shown to efficiently describe shape variation of *Palmatolepis* elements (Renaud and Girard 1999; Girard and Renaud 2012). The zero harmonic A0, proportional to the outline size, was used to standardize all other FCs so they correspond to shape variables only. The higher the rank of the harmonics, the more details they represent on the outline; this usually goes with an increasing amount of measurement error (Crampton 1995; Renaud et al. 1996). The first nine harmonics, i.e. 18 variables, were considered to provide a good balance between a satisfying description of the geometry of the element, and an efficient filtering of measurement error.

Multivariate shape analysis. – The total shape variance can be mathematically described by the **T** matrix, corresponding to the variance-covariance (VCV) matrix of the standardized 18 FCs x 1435 specimens. A Principal Component Analysis on **T** was performed to display the total shape variance on few synthetic axes maximizing the total variance.

T can be decomposed in two components: the between-group matrix **B** and the within-group matrix **W** (**T = B+W**), the groups being here the OTUs. **B** corresponds to the VCV matrix between group means weighted by the sample size of each group. Its eigenanalysis is termed between-group

Principal Component Analysis (bgPCA) (Culhane et al. 2002; Renaud et al. 2015). Here, a bgPCA was performed to characterize the shape differentiation between OTUs.

Pmax, allometry, and correlations between vectors. – The shape variance within a OTU is described by the VCV matrix of the Fourier coefficients of the specimens composing the OTU (P-matrix). A PCA on this P-matrix leads to a set of eigenvectors characterizing directions of variance within the OTU. The first eigenvector (Pmax) describes the direction on which most shape variance occurs. The comparison of Pmax between two OTUs allows to assess if they share similar patterns of main variance. The correlation (R) between Pmax in OTU1 and OTU2 corresponds to the inner-product of the two vectors scaled to unit length. The angle between the two vectors corresponds to the arccosine of R. The significance of the correlation was assessed by comparing the observed R value to a null distribution of R between random vectors of 18 dimensions and a randomly chosen fixed reference direction; this null distribution was generated by computing 10,000 correlations (Renaud et al. 2006; Hunt 2007). Since the +/- direction of principal axes is arbitrary, the absolute value of R was considered. For the significance levels (type I error) alpha = 0.05, 0.01 and 0.001, the obtained $|R_{observed}|>|R_{random}|$ are respectively $|R|=0.457$ (angle=62.8°); $|R|=0.588$ (angle=45.0°); and $|R|=0.699$ (angle=45.6°).

The vectors describing the allometric shape variation were estimated using the slope coefficients of multiple regressions of the 18 FCs vs A0 (zero harmonic), performed separately for each OTU. The resulting vectors were scaled to unit length and their correlations were assessed as described above.

Correlations between P matrices. – The RV coefficient is defined as the sum of the squared covariances between two sets of variables, divided by the total amount of variation in the two sets of variables (Escoufier 1973). The RV coefficient varies between 0 and 1 and it can be seen as an extension of the notion of correlation for matrices. The significance of the correlation was assessed for each pair of P-matrices using permutations (9999 permutations).

Another metric was used to compare P-matrices, based on the contrast defined as the square root of the summed squared logarithms of the relative eigenvalues between the two matrices. Relative eigenvalues express the variances and covariances of one sample relative to that of another sample; they are equal to the eigenvalues of the product of one matrix premultiplied by the inverse of the other matrix (Mitteroecker and Bookstein 2009). The resulting matrix of “MB” contrasts (for the

initial of the authors describing it) summarized the distances between P-matrices of the different OTUs.

Multivariate analyses of distances between vectors and matrices. – Distance matrices can be decomposed using Principal Coordinate Analyses (PCOA) in order to summarize the relationships between items on few synthetic axes. Such an approach can be used to characterize relationships between vectors (Pmax, allometry) or P-matrices, provided that Euclidean distances between OTUs matrices can be calculated.

For this purpose, the matrix of correlation between Pmax vectors was transformed into a matrix of Euclidean distances using the formula: $d = \sqrt{(2*(1-R^2))}$ (Qannari et al. 1998); the same procedure was used for allometric vectors. The table of RV coefficients between P-matrices was transformed into a matrix of distances using the formula $d = \sqrt{(2*(1-RV))}$ (Robert and Escoufier 1976). The matrix of MB contrasts being itself a distance matrix, it could be analyzed by a PCOA without further transformation.

Comparison of evolutionary trajectories with Pmax and allometric vectors. – Evolutionary trajectories were defined as directions of shape changes between two groups. Trajectories characterizing the differentiation between subgenera were evaluated as the pairwise differences between the mean shape of the different subgenera. Trajectories of within-subgenus evolution were estimated as the difference between the mean shape of the oldest and most recent OTU within each subgenus. This provided six between-subgenera and four within-subgenus trajectories. In order to assess whether evolutionary changes were channeled along directions of within-OTU variation, the between-subgenera and within-subgenus trajectories were compared to the direction of main variance (Pmax) and to the allometric direction of all OTUs. This was done by estimating the correlation of the evolutionary trajectories, scaled to unit length, with the Pmax and the allometric vectors of the 22 OTUs.

An integrated analysis of shape and shape variance: a K-table approach. – The 22 OTUs were characterized using descriptors of different formats: mean shape; vectors describing directions of shape variation for Pmax and allometry, and P-matrices describing the structure of the variation. For each descriptor, the relationship between the 22 OTUs was assessed using a multivariate analysis (bgPCA or PCOA), raising the question of how the resulting topologies related with the others. The

match between pairs of topologies was assessed using a Protest (Peres-Neto and Jackson 2001), providing a coefficient of correlation (ProcR) and a P-value, estimating if the configurations are more related than random (based on 9999 permutations). The first three dimensions of all multivariate analyses were considered for these pairwise tests.

Multivariate methods exist to compare the analyses of several tables sharing the same entries ("K-tables" approaches). Among them, the DISTATIS method (Abdi et al. 2005) was designed for the simultaneous analysis of multiple distance matrices, allowing to integrate them into a single graphical representation. It was thus applied here to the five distance matrices describing the topology between the 22 conodont OTUs. This approach provides a set of compromise eigenvectors on which the five descriptors of the 22 OTUs are projected; this therefore allows a visualization of which descriptors provide the most similar patterns of differentiation between the 22 OTUs. The method further allows a bootstrap estimate of the position of the OTUs on this compromise. 1000 bootstraps were performed here.

Assessment of shape variation due to asymmetry. – All OTUs except PAN_51 included both right and left elements. To assess if asymmetry could be an important driver of morphological variation, two approaches were explored. First, the relative importance of the potential sources of variation (subgenus or OTU, bilateral asymmetry and allometry) was estimated using a multivariate analysis of variance on the set of FCs using the "ffmanova" procedure (Langsrud and Mevik 2012). This method has the advantage of being invariant to ordering of the model terms and to handle colinear responses. It may inflate the percentage of variance explained (pve) but allows an estimation of the relative importance of the explanatory variables.

Second, the same multivariate analyses (bgPCA, PCOA based on Pmax and on the RV coefficients between P-matrices) as described above were performed on the sub-sample including right elements only. The analyses based on MB contrasts and allometry could not be performed because in few OTUs, the sample size was inferior to the number of variables (Table 1). The between-OTUs topologies obtained for shape (bgPCA), Pmax and P-matrices based on all elements, and right elements only, were compared using Protest on the first three axes.

Visualization of shape variation. – The outline corresponding to a set of FCs can be visualized using an inverse Fourier transform. For Pmax, the outlines corresponding to the 10% and 90% percentiles of the scores along the vector of each OTU were reconstructed. For allometry, outlines corresponding

to the 10% and 90% percentiles of the size distribution were computed using the same multivariate regressions that provided the coefficients of the allometric vector.

The P-matrices were represented by ellipses defined by their first and second axes, providing a representation of the orientation and elongation of each matrix. To be comparable, all matrices had to be projected on a common space, here the space of the PCA on the total sample.

Finally, the temporal changes in mean shape, Pmax, P-matrices, and allometry, were visualized as the scores of the OTUs along the first axis of the different multivariate analyses, as a function of geological time, based on the age model relating depth along the section to absolute age (Girard et al. 2020) and updated according to the most recent datation framework (Becker et al. 2020). To provide an environmental background to these morphological variations, paleotemperature estimates based on $\delta^{18}O$ values measured on conodont apatite from the same samples (Girard et al. 2020) were also represented.

Packages and data accessibility. – All analyses were performed under R (R_Core_Team 2017). Multivariate analyses were performed using ade4 (Dray and Dufour 2007; Thioulouse et al. 2018) and DistatisR (Beaton et al. 2019). Protests were performed using vegan (Oksanen et al. 2017) and ffmanova using the ffmanova package (Langsrud and Mevik 2012). The R script and the dataset are deposited in Dryad: https://doi.org/10.5061/dryad.pvmcvdnmf.

Results

Shape differentiation between and within conodont subgenera. – Considering the analysis of the total shape variance using a PCA (Fig. 2A), the prominent morphological signal was the difference between elements with a well-developed platform, typical of *Manticolepis* and *rhomboidea*, and slender elements without a platform, characteristics of *Deflectolepis* (Fig. 2B). The subgenus *Panderolepis* appears as intermediate between the two extreme morphologies. The second axis does not differentiate subgenera, but it expresses within- and between-group variation within *Deflectolepis*.

Between-group differences, as summarized by a bgPCA (Fig. 2C), represent 68.2% of the total variance. The first axis is overwhelmingly important (86.2% of the between-group variance) and matches the signal expressed on the first axis of the PCA (difference between elements with a well-developed platform and those without a platform). *Panderolepis* is intermediate between

Manticolepis and *Deflectolepis* along bgPC1, but its OTUs are ordered according to a temporal sequence: the oldest OTUs (PAN_35 and PAN_37) are close to *Manticolepis* while the most recent OTU (PAN_56) is close to *Deflectolepis*. Furthermore, *Panderolepis* is slightly differentiated from the other subgenera along bgPC2 (6.7% of between-group variance).

Differences between Pmax vectors. – The correlation between the Pmax vectors varies greatly depending on the OTUs considered (Supp. Table 1). It is higher when comparing OTUs from a same subgenus (mean R=0.797) than when the comparison involves different subgenera (mean R=0.467). Pmax is particularly stable within *Deflectolepis* (mean R = 0.960) and *rhomboidea* (mean R=0.925). It varies more within *Manticolepis* (mean R = 0.705) but this is especially due to the outlying direction of the earliest OTU (MAN_06). When focusing on later *Manticolepis* OTUs (from MAN_07 to MAN_23), Pmax is also stable through time (mean R = 0.909). Pmax is the more variable within *Panderolepis* (mean R=0.612), due to the outlying direction of the two early OTUs, especially PAN_37. It is stable within the three late *Panderolepis* OTUs (mean R=0.943).

The main axis of the ellipses corresponding to the projection of the P-matrix provides a visualization of the Pmax direction (Fig. 3A). According to the high within-subgenus correlation, Pmax is stable within *Deflectolepis*. The ellipses vary more in their orientation and elongation in *Panderolepis*. Especially, an inversion of the first and second axes is observed in PAN_37. In *Manticolepis*, Pmax shifts from being aligned with PC2total to being almost aligned with PC1total. The elongation of the ellipse characterizes the anisotropy of the variance. As shown by the elongated ellipses, *Deflectolepis* is characterized by a very anisotropic variance, with Pmax representing 50% or more of the variance in all OTUs (Supp. Fig. 2A).

Extreme outlines along each Pmax provides a visualization of the shape variance within each sample (Fig. 3B). In *Manticolepis*, Pmax corresponds to a variation between pear-shaped elements and elements with a pronounced lobe. MAN_06 constitutes an exception, with a variation from straight to arched elements, without noticeable variation in the extension of the lobe. In *rhomboidea*, the extension of the platform varies little and Pmax corresponds to a variation between more or less sigmoidal carina. In *Deflectolepis*, Pmax expresses a variation from straight to curved elements. This kind of variation is also characteristics of *Panderolepis*; however, in the oldest samples PAN_35 and PAN_37, a small lobe is still present. Variation of its extension is predominant over the change in rectitude in PAN_37.

A multivariate analysis (PCOA based on the correlations between Pmax scaled to unit length, converted into distances) summarized the relationships between all Pmax (Fig. 4A). The resulting

364 topology was correlated to the pattern of the bgPCA (Table 2). As for the analysis of shape,
365 *Manticolepis* (to the exception of MAN_06) is opposed to *Deflectolepis* along the first axis. In contrast
366 to the analysis of shape, however, *Panderolepis* OTUs (to the exception of PAN_37) fall with
367 *Deflectolepis*, and *rhomboidea* is clearly apart along $PC2_{Pmax}$. The outlying position of PAN_37
368 compared to other *Panderolepis* samples is due to the inversion between the first and second main
369 directions of variance (see Fig. 3A, 3B), corresponding to the relative extension of the lobe, and the
370 curvature of the element. The similarity of PAN_37 Pmax with *Manticolepis* Pmax is attributable to
371 the fact that they all describe variation in the extension of the lobe. The outlying position of MAN_06
372 is due to the curvature, and not the extension of the lobe, being the prominent component of shape
373 variance.

374

375 Comparison of the P-matrices. – A first approach to compare P-matrices was based on the RV
376 coefficient, that provides a measure of correlation between two matrices (Supp. Table 2). P-matrices
377 are highly correlated among OTUs of a same subgenus, with particularly high correlations within
378 *Deflectolepis* and *rhomboidea* (RV>0.8, P=0.0001). This is also the case for *Manticolepis* when
379 discarding MAN_06, which P-matrix is less tightly related to the P-matrices of the other OTUs (0.5<
380 RV< 0.9). P-matrices are more variable within *Panderolepis* (RV>0.6). In contrast, P-matrices are not
381 always significantly correlated between subgenera, especially when comparing *Deflectolepis* and
382 *Manticolepis* (all RV<0.6).

383 A PCOA was applied to the distance matrix derived from this table of RV coefficients (Fig. 4B). The
384 general pattern resembles the one provided by the multivariate analysis of Pmax and by the bgPCA
385 (Table 2). However, the differentiation between subgenera appears less important than in the Pmax
386 analysis. The first axis once again contrasts *Manticolepis* to *Deflectolepis*, showing that the two
387 subgenera have a different structure of morphological variance. In *Manticolepis*, most variance
388 occurs on the lobe, whereas in *Deflectolepis*, the prominent component of variance involves the
389 curvature of the elements. *Panderolepis* OTUs scatter in intermediate positions; the oldest samples
390 PAN_35 and PAN_37 are closer to *Manticolepis* and the more recent PAN_50, PAN_51 and PAN_56
391 are closer to *Deflectolepis*. The second axis differentiates *rhomboidea* from the three other
392 subgenera. Note that when considering Pmax (Fig. 4A), MAN_06 and PAN_37 were outliers
393 compared to other OTUs of the same subgenus. Their position in the PCOA space based on RV
394 coefficients between P-matrices is more in agreement with their subgeneric attribution.

395 The P-matrices were also compared using the MB contrast (Mitteroecker and Bookstein 2009) (Fig.
396 4C), providing a topology close to the one obtained based on the RV coefficients (Table 2). The first

axis is similar to the axis based on RV coefficients. The difference regards the second axis isolating *Panderolepis* instead of *rhomboidea*. The discrepancy between the PCOAs based on RV coefficients and MB contrasts comparing the same P-matrices is due to an inversion of the second and third axes between the two analyses (Supp. Figure 3). Overall, the MB analysis of the P-matrices provides a topology close to those based on mean shape, Pmax and especially on the RV coefficients between P-matrices, and showed a good congruence of the two descriptors of the relationships between P-matrices (Table 2).

Allometry. – Size variation is comparatively high in *Manticolepis* and *Panderolepis* (5%-95% range=1.93 for *Manticolepis* and 1.97 for *Panderolepis*), low in *rhomboidea* (range=1.37) and the lowest within *Deflectolepis* (range=1.26) (Fig. 5). Multiple regression of the FCs vs A0 was significant in all groups except DEF_56 (Supp. Figure 2C); it was the highest in RHO_39. Allometry involves weak shape changes compared to the variation along Pmax (Fig. 3C). In *Manticolepis*, growth is associated with an expansion of the lobe. In *rhomboidea*, the free blade becomes more apparent. In *Panderolepis*, elements tend to become slender and more arch-shaped. Allometric change is very tenuous in *Deflectolepis*, up to the absence of any change in DEF_56. The coefficients of the multiple regressions between size (A0) and shape (FCs) within each OTU allowed to characterized 22 allometric vectors. Being scaled to unit length, their pairwise correlations were assessed (Supp. Table 3). Allometric vectors were weakly correlated among subgenera (mean R=0.023) and within *Deflectolepis* (mean R=0.208). They were moderately related within *Panderolepis* (mean R=0.650) except for the three latest OTUs (R>0.85). Allometric vectors were highly correlated within *Manticolepis* (mean R=0.833) and especially within *rhomboidea* (all R>0.85). Allometric vectors were further compared to Pmax for each of the 22 OTUs, all vectors being scaled to unit length (Supp. Table 4). Hardly more than 10% of the correlations were significant at the significance level alpha = 0.001. The only exceptions to this weak relation were the late *Manticolepis* (MAN_22 and MAN_23) and especially *rhomboidea* (|R|>0.8).

The relationships between allometric vectors (scaled to unit length) were summarized using a PCOA (Fig. 4D). The resulting pattern is significantly correlated with those obtained based on Pmax and P-matrices (Table 2; Fig. 4A, B, C). *Manticolepis* allometric vectors clustered towards positive values along the first axis. *Panderolepis* and *rhomboidea* shared negative values along the first axis but were different along the second axis. *Deflectolepis* allometric vectors were scattered along the first and second axes. The weak allometric signal probably made its estimation unstable across OTUs.

Evaluation of asymmetry as a source of shape variation. – The linear models indicated that asymmetry explained less than 0.6% of shape variance in all cases (Table 3), much less than size and temporal variation through the successive levels. The effect was however significant in *Manticolepis, Panderolepis* and *Deflectolepis*, probably due to the large sample size.

The topologies based on all elements and right elements only were highly correlated when considering shape (bgPCA: ProcR = 0.9963, P = 0.0001), Pmax (ProcR = 0.9090, P = 0.0001) and P-matrices compared using RV coefficients (ProcR = 0.9743, P = 0.0001). Further note that the OTU DEF_51, sampled by right elements only, never emerged as an outlier.

Evolutionary trajectories and directions of shape variance. – Evolutionary trajectories characterizing shape changes between subgenera and ancestor-descendent changes within each subgenus were compared to the Pmax and allometric vectors of the 22 OTUs, all vectors being scaled to unit length (Supp. Table 5; Supp. Figure 4). Trajectories between subgenera were poorly related to Pmax (mean R=0.337) and to allometric vectors (mean R=0.414). Nevertheless, the differentiation between the Frasnian *Manticolepis* and the three Famennian subgenera (*Deflectolepis, Panderolepis*, and *rhomboidea*) was moderately related (mean R=0.680) to the direction of Pmax in the late *Manticolepis* (MAN_11c to MAN_23).

The within-subgenus evolutionary trajectories were more strongly related to the Pmax direction within the involved subgenus (mean R=0.675), but not to the allometric direction of shape change (mean R=0.325). The match between the ancestor-descendent shape change and Pmax was particularly strong within *Deflectolepis* (mean R=0.951). It was also strong within *Manticolepis* (mean R=0.651), especially when focusing on OTUs posterior to MAN_06 (mean R=0.751). The relationship was moderate within *rhomboidea* (mean R=0.614) and low within *Panderolepis* (mean R=0.358).

An integrated analysis of shape, Pmax, allometry, and P-matrices. – Five descriptors characterized the differences between the 22 OTUs: shape, main direction of shape variance (Pmax), structure of shape variance (P-matrices compared using RV coefficients and MB contrasts), and allometric vectors. This resulted in five topologies of the 22 OTUs on multivariate axes. These topologies shared some features, for instance the important differentiation between *Manticolepis* and *Deflectolepis*, and in agreement, these topologies were significantly related according to the Protests. Nevertheless, they also differed in important aspects, especially regarding the position of *Panderolepis* and *rhomboidea* relative to the two other subgenera.

462 The DISTATIS method allowed for the simultaneous analysis of these five descriptors. Despite being
463 different in nature (set of Fourier coefficients, vectors, and matrices), the relationships between the
464 22 OTUs based on the five descriptors were comparable, being expressed as Euclidean distance
465 matrices. The five descriptors shared positive loadings on the first axis of the compromise space of
466 the DISTATIS analysis (Fig. 6A), underlining that the topologies based on mean shape, Pmax, P-matrix
467 and allometry are related (see Table 2). Yet, allometry diverged from the other descriptors along the
468 second axis of the compromise space. Shape, Pmax and the RV comparisons between the P-matrices
469 provided the closest results.

470 On the same compromise first plane, the pattern of differentiation between the 22 conodont OTUs
471 provided by the five descriptors allows to recognize similitudes and discrepancies (Fig. 6B).
472 *Manticolepis* and *rhomboidea*, very close in shape, display distinct P-matrices and even more distinct
473 allometric directions, since they are the most divergent along the second axis. The samples MAN_06
474 and PAN_37, diverging from their subgenus for shape and Pmax, clearly display P-matrices and
475 allometric direction in agreement with their subgeneric attribution.

476 As a result, the compromised position of the different groups is very coherent with their subgeneric
477 identification (Fig. 6C). Samples attributed to a same subgenus are clustered on the compromise
478 space, and bootstrap estimates show that their position is robust regarding sampling issues.
479 *Panderolepis* is the most variable, its oldest representative (PAN_35 and PAN_37) being close to
480 *Manticolepis*, typical of the Frasnian, while more recent samples are close to *Deflectolepis*, typical of
481 the Late Famennian.

482

483 Temporal changes of shape and shape variance. – The temporal changes of the five descriptors can
484 be visualized as the scores of the 22 OTUs on the first axis of the different multivariate analyses, as a
485 function of geological time (Fig. 7). Mean shape (Fig. 7A) shows an opposition between *Manticolepis*
486 and *rhomboidea* and Late Famennian *Deflectolepis*. *Panderolepis* shifts from shapes plotting towards
487 *Manticolepis* (PAN_35 and PAN_37) to shapes close to *Deflectolepis*. During the Late Frasnian record,
488 *Manticolepis* displays a slight reduction of its platform, leading to a shift towards less extreme scores
489 along the shape axis.

490 All the descriptors of shape variance (Pmax and P-matrices) share similar features (Fig. 7B, C): major
491 difference between *Manticolepis* and *Deflectolepis*, stability in *Deflectolepis*, temporal changes
492 within *Manticolepis* and *Panderolepis*, with the oldest samples (MAN_06 for *Manticolepis* and
493 PAN_35 and/or PAN_37 for *Panderolepis*) diverging from the most recent samples. MB contrasts
494 between VCV matrices insist on the intermediate position of *Panderolepis* between *Manticolepis* and

Deflectolepis. The idiosyncrasy of *rhomboidea* variance pattern does not appear on these representations, because it is always expressed on the second or third multivariate axis; along the first axis, *rhomboidea* shares similar scores with the other subgenus with a well-developed platform, *Manticolepis*. Allometry (Fig. 7D) provides a different picture, with *Manticolepis* being most different from *rhomboidea* and *Panderolepis*. All subgenera display a temporal stability in their pattern of allometric variation, except for *Deflectolepis*. Variation in the allometric pattern within this subgenus is however attributable to the weak signal preventing a robust estimate of the direction of allometric shape change, if any.

A paleoenvironmental background was provided by temperature estimates based on oxygen isotope values derived from conodont apatite (Fig. 7E). Rapid and pronounced temperature changes occurred during the Late Frasnian, followed by environmental stability during the beginning of the Famennian, and a subsequent step-wise temperature decrease.

Discussion

Remodeling of the P-matrices: a tracer of changes in functional constraints?

The most striking result of the present study was that long-term morphological evolution, leading from conodont elements with a well-developed platform to slender elements, was associated with deep changes in the pattern of shape variance. This was observed both as a temporal trend along the Famennian, and in the diversification among subgenera. Shapes with a large platform were associated with a variance concentrated on the relative development and morphology of this platform, whereas in groups with a reduced platform, variance corresponded to the curvature of the carina. Allometry was never found to be a main component of morphological variance, but its contribution considerably varied among subgenera. In those with a well-developed platform (*Manticolepis* and *rhomboidea*), allometry represented more than 10% of shape variance and involved changes in the shape and extension of the platform. In subgenera with a reduced platform, allometry represented less than 5% of shape variance, since the relative development of an anyway reduced platform did not constitute an important morphological signal.

The 2D projection of the platform shape provided a good approximation of 3D morphological changes in a related taxon, *Polygnathus* (Renaud et al. 2021), belonging as *Palmatolepis* to the Ozarkodinida Order (Donoghue et al. 2008). Such 2D simplification allows an extensive sampling, and thus the quantification of variance patterns through time; it however provides only indirect information about the three-dimensional geometry of the elements (Fig. 8) and thus about the

functional constraints related to their occlusion. *Manticolepis* elements had a well-developed platform (Fig. 8A), but most of it could not come into contact with the platform of the opposite element (Nicoll 1987). Contact between occluding elements should thus have been concentrated along the blades (Donoghue 2001). The large and almost flat platform may have served as anchorage into the soft tissues of the jawless mouth. In contrast, in most recent *Deflectolepis* (Fig. 8D), the platform was absent and therefore could not vary in shape; the blade and carina were the most prominent features of the elements. The angle in the blade-carina alignment contributed most to the morphological variance in this subgenera and most probably, it constrained the way the two elements went into occlusion. Characterized by a reduced but still present platform, *Panderolepis* elements (Fig. 8C) displayed a shape marked by an elevated inner anterior platform edge ("shoulder") up to the development of a parapet, delineating a groove of varying depth between the blade and the border of the inner platform. The opposite blade, when coming into contact, should thus have been stabilized along this groove, as observed in *Polygnathus* (Martínez-Pérez et al. 2016). The shape changes associated with Pmax and the P-matrix in this subgenus (Fig. 3) suggested that the main component of variance, corresponding to more or less sigmoidal shapes, expressed more or less pronounced shoulder and parapet. Note that asymmetry was never found important in *Palmatolepis* elements, being one order of magnitude less that what has been found in *Polygnathus* (Renaud et al. 2021). Asymmetry was the less pronounced in the subgenera with a large platform, corroborating that the opposite platforms had few functional interactions in these morphologies. The profound remodelling of the P-matrices among subgenera therefore illustrates that important changes in mean shape involved modifications in the functional constraints, in turn conditioning what kinds of morphological variants could be realized within a population.

The shift of *Palmatolepis* mean shape along the Famennian, leading from elements with to elements without well-developed platform, observed even when considering whole assemblages (Girard and Renaud 2012), suggests that the adaptive optimum shifted in favor of slender elements devoid of platform. It does not relate to evident abiotic changes, since the first half of the Famennian was a rather stable period (Girard et al. 2020). The cooling characterizing the mid-Late Famennian postponed the shift towards a reduction of the *Palmatolepis* platform. It could be rather related to a rearrangement of the nektonic fauna, with the expansion of potential competitors and predators of conodonts, such as sharks and bony fishes (Ginter et al. 2002; Gauchey et al. 2014), leading to new functional constraints on the feeding apparatus.

Response of P-matrices to short term environmental fluctuations and evolutionary consequences

The Latest Frasnian was a period of intense environmental perturbations. Temperature abruptly dropped towards the end of the LKE (Girard and Renaud 2007), and progressively increased again between the LKE and the UKE (Fig. 7) before a second rapid temperature decrease during the UKE, culminating with the F/F crisis (McGhee 1996; Joachimski and Buggisch 2002). A morphological response was documented in *Palmatolepis*, with changes in mean shape tracking temperature variations during the Latest Frasnian, leading to a back- and forth evolution of larger platform when temperature decreased (e.g., end of the LKE) and narrower platforms when temperature increased (Balter et al. 2008). Temperature changes were associated with productivity variations, suggesting that the paleoenvironmental perturbations had profound effects on the trophic chains (Balter et al. 2008), thus probably exerting strong selective pressure on the feeding apparatus of the conodont animal. The reorientation of Pmax and P-matrix documented between MAN_06 and the following *Manticolepis* OTUs illustrates their remodeling following a moving peak optimum (Eroukhmanoff 2009; Jones et al. 2012). Such reorientation can boost evolutionary responses to environmental changes (Hangartner et al. 2019). It may have been a key to the successful response to the even more rapid and drastic environmental changes marking the UKE and the F/F crisis. Most if not all Famennian representatives are supposed to be derived from Frasnian *Manticolepis* (Helms and Ziegler 1981). The divergence in mean shape leading from *Manticolepis* to the Famennian subgenera *rhomboidea*, *Panderolepis* and *Deflectolepis* occurred along the Latest Frasnian *Manticolepis* Pmax, showing that the Famennian diversification surfed on the variance in platform shape that resulted from the response to the environmental perturbations during the LKE-UKE interval.

Patterns of variance within subgenera: contrasted evidences

In contrast with these reorientation of the P-matrices following moving adaptive optima, Pmax and P-matrices were stable within two subgenera, *Deflectolepis* and *rhomboidea*. The temporal extension of the latter is quite short in our sampling (less than 0.5 myrs), letting little time for changes in the pattern of variance; this nevertheless represents a substantial part of the temporal extension of this short-lived group. The temporal range covered by the *Deflectolepis* OTUs was in contrast 5 myrs long. This suggests that these subgenera remained close to a stable adaptive optimum, retaining the same functional constraints and the same patterns of variation. Accordingly, the morphological evolution from early to late *Deflectolepis* was of moderate magnitude and occurred according to Pmax, suggestive of stabilizing or weak directional selection. In such cases, the constraints embodied in the P-matrix are prone to channel morphological evolution (Ackermann and Cheverud 2004; Renaud et al. 2006).

593 In contrast, Pmax and P-matrices were found to vary within the ~3.5 myr record of *Panderolepis*. This
594 may be due to species replacement, with *tenuipunctata* occurring in the first two OTUs (PAN_35 and
595 PAN_37) whereas *glabra* is the sole species in the later OTUs. Shape, Pmax and P-matrices of
596 *Panderolepis* OTUs dominantly composed of *tenuipunctata* share similarities with *Manticolepis* OTUs,
597 whereas later OTUs share more similarities with *Deflectolepis*. *Panderolepis* may document, at the
598 micro-evolutionary level, the trend of platform reduction also expressed at the macro-evolutionary
599 level among subgenera and among whole assemblages (Girard and Renaud 2012), confirming a
600 general shift in the adaptive optimum during the Famennian, and that the reduction of the platform
601 was associated with a reorientation of the P-matrices, pointing to new constraints on morphological
602 variation. Nevertheless, all *Panderolepis* samples, being composed of *tenuipunctata* or *glabra*, share
603 common features of the P-matrix (Fig. 4C) and allometry (Fig. 4D), showing homogeneity despite the
604 shape changes characterizing the Famennian record of this subgenus.

605 Patterns of allometric growth were very stable within *Manticolepis* and *rhomboidea* as well. In
606 contrast, the allometric pattern varied within *Deflectolepis*, but this was due to the little amount of
607 allometric variation. Despite of the stable allometric pattern characterizing most of the subgenera,
608 allometry did not constitute a line of least evolutionary resistance in *Palmatolepis*. This suggests that
609 the basic shape of each element was determined by the shape of the initial nucleus, later on only
610 moderately modified by differential accretion. This also suggests that functional constraints did not
611 deeply changed through age, but remained relatively stable through ontogeny.

612

613 *P-matrices through time: stability and changes as a response to moving adaptive optimum*

614 The study of G/P-matrices in modern organisms delivered contrasted results, with both evidences of
615 short-term fluctuations (Roff and Mousseau 2005; Guillaume and Whitlock 2007; Eroukhmanoff and
616 Svensson 2008) and stability (Bégin and Roff 2003; McGuigan et al. 2005). The nature of the traits
617 probably influences the results: demographic traits, which may vary rapidly due to differences in
618 acquisition/allocation patterns, may be more prone to show rapid variations of the P-matrix
619 (Björklund et al. 2013). Estimates of Pmax and P-matrix in the fossil record are still uncommon, and
620 inevitably raise some issue with time-averaging. However, it seems to have little impact on estimates
621 of trait variation (Hunt 2004). If ever, it may buffer short-term variations, as it does for evolutionary
622 rates (Gingerich 1983).

623 Few studies delivered insights into the temporal stability of Pmax over a duration similar to the
624 *Palmatolepis* record considered here (~10 myrs). In two related lineages of Late Triassic conodonts,
625 Pmax was found to be stable over such a time period (Guenser et al. 2019). In murine rodent molars,

Pmax was also found to be stable along evolutionary lineages and across phylogenetic divergence over 10 myrs (Renaud et al. 2006; Renaud and Auffray 2013). In contrast, in ostracod shells, the correlation between Pmax of successive OTUs was found to fade away over few million years (Hunt 2007). Compared to these records, the subgenus *Palmatolepis* delivered both examples of mid-term stability and of rapid remodeling of the P-matrix. Contrary to subgenera such as *Manticolepis* and *Deflectolepis*, being differentiated by the size of their platform, the Late Triassic conodont lineages shared close morphologies and they probably shared similar constraints regarding occlusal functioning, explaining the conserved pattern of variance. In murine rodents, important modifications occurred on the molar teeth along the 10 myrs of evolution, such as the addition of new crests, and the broadening and heightening of the molars (Renaud et al. 2005). Nevertheless, the typical mastication for murine rodents was not modified (Lazzari et al. 2008), maintaining similar strong functional constraints on the alignment of molar cusps. In contrast, functional constraints on ostracod shells may be less strong, being related to the physical properties of the aquatic habitat, or to anti-predator defenses, letting more latitude for changes of the variance pattern along time and phyletic evolution. Therefore, stability or changes in P-matrices over time could deliver insights into the strength of functional constraints and their persistence or change along morphological evolution. Our results also provide empirical evidences that moving adaptive optima indeed cause a reorientation of the variance pattern by selecting new phenotypic variants (Eroukhmanoff 2009). In this context, one strength of the present study is to have quantified not only Pmax but P-matrices through time. Considering P-matrices provides a more complete assessment of the patterns of variance-covariance and more nuanced insights into temporal changes, because P-matrices are less impacted by instability between the first (Pmax) and second axes of morphological variance.

Conclusion

Beyond the study of mean shape, evaluating Pmax and P-matrices through time may thus shed light on the response of species to changing environments and/or functional constraints. On time scales of several millions of years, the question seems not to be whether the P-matrix is stable, but how it is varying in response to changes in selection regimes and shifts in adaptive optimum. Our study validated the hypothesis that environmental fluctuations impacting the faunas, likely representing moving adaptive optima, selected for new mean shapes but also for new types of variants around mean shape, thus reorienting Pmax and the P-matrix. We also validated the hypothesis that during periods of relatively stable environmental conditions, Pmax and P-matrix were conserved and channeled the moderate evolution in mean shape within subgenera. In contrast, we did not validate

allometry as a major component of shape variance in *Palmatolepis*, suggesting that heterochronic processes were not important in the diversification of buccal elements within this genus. Instead, evolution in mean shape seems related to changes in occlusal functioning, switching from a scissor-like contact between blades stabilized by a large platform in *Manticolepis*, to an occlusion stabilized by an inner shoulder up to a parapet in *Panderolepis*, or a reduction to mere occluding blades in *Deflectolepis*. By changing the functional constraints, this evolution involved changes in the realized variance around mean shape, traduced by a reorientation of Pmax and the P-matrices. In such deep times and with such fossil groups devoid of modern equivalents, the study of stability and changes in morphological variance may help, beyond the study of mean shape alone, to characterize moving adaptive optima, and functional constraints related to a given geometry.

Conflict of interest

The authors declare that they have no conflict of interest.

Acknowledgements

We warmly thank Anne-Lise Charruault for her help in acquiring a part of the pictures of the conodont elements. We also thank the anonymous reviewers whose constructive comments on successive versions of the manuscript significantly contributed to improve the final version. This work was supported by the ECODEV grant ANR-13-BSV7-005. This is publication ISEM XXXX-XXX.

References

Abdi, H., D. Valentin, A. J. O'Toole, and B. Edelman. 2005. DISTATIS: the analyse of multiple distance matrices. Pp. 42-47 *in* P. o. t. I. C. Society, ed. International Conference on Computer Vision and Pattern Recognition, San Diego, CA, USA.

Ackermann, R. R. and J. M. Cheverud. 2004. Detecting genetic drift versus selection in human evolution. Proceedings of the National Academy of Sciences, USA 101:17946-17951.

Aldridge, R. J., M. P. Smith, R. D. Norby, and D. E. G. Briggs. 1987. The architecture and function of Carboniferous polygnathacean conodont apparatus. Pp. 63-76 *in* R. J. Aldridge, ed. Palaeobiology of conodonts. Ellis Horwood, Chichester, England.

Arnold, S. J., M. E. Pfrender, and A. G. Jones. 2001. The adaptive landscape as a conceptual bridge between micro- and macroevolution. Genetica 112-113:9-32.

Balter, V., S. Renaud, C. Girard, and M. M. Joachimski. 2008. Record of climate-driven morphological changes in 376 Ma Devonian fossils. Geology 36:907-910.

693 Beaton, D., C. C. Fatt, and H. Abdi. 2019. DistatisR: DISTATIS. Three way metric multidimensional
694 Scaling. , https://CRAN.R-project.org/package=DistatisR.
695 Becker, R. T., J. E. A. Marshall, A.-C. Da Silva, F. P. Agterberg, F. M. Gradstein, and J. G. Ogg. 2020.
696 Chapter 22 - The Devonian Period. Pp. 733-810 *in* F. M. Gradstein, J. G. Ogg, M. D. Schmitz,
697 and G. M. Ogg, eds. Geologic Time Scale 2020. Elsevier.
698 Bégin, M. and D. A. Roff. 2003. The constancy of the **G** matrix through species divergence and the
699 effects of quantitative genetic constraints on phenotypic evolution: a case study in crickets.
700 Evolution 57:1107-1120.
701 Beldade, P., K. Koops, and P. M. Brakefield. 2002. Developmental constraints versus flexibility in
702 morphological evolution. Nature 416:844-847.
703 Björklund, M., A. Husby, and L. Gustaffson. 2013. Rapid and unpredictable changes of the G-matrix in
704 a natural bird population over 25 years. Journal of Evolutionary Biology 25:1-13.
705 Bonhomme, V., S. Picq, C. Gaucherel, and J. Claude. 2014. Momocs: Outline Analysis Using R. Journal
706 of Statistical Software 56:1-24.
707 Cardini, A. and S. Elton. 2007. Sample size and sampling error in geometric morphometric studies of
708 size and shape. Zoomorphology 126:121-134.
709 Chen, Y., T. A. Neubauer, L. Krystyn, and S. Richoz. 2016. Allometry in Anisian (Middle Triassic)
710 segminiplanate conodonts and its implications for conodont taxonomy. Palaeontology
711 59:725-741.
712 Cheverud, J. M. 1988. A comparison of genetic and phenotypic correlations. Evolution 42:958-968.
713 Crampton, J. S. 1995. Elliptic Fourier shape analysis of fossil bivalves: some practical considerations.
714 Lethaia 28:179-186.
715 Culhane, A. C., G. Perrière, E. C. Considine, T. G. Cotter, and D. G. Higgins. 2002. Between-
716 groupanalysisofmicroarray data. Bioinformatics 18:1600-1608.
717 Donoghue, P. C. 2001. Microstructural variation in conodont enamel is a functional adaptation.
718 Proceedings of the Royal Society of London, Biological Sciences (serie B) 268:1691-1698.
719 Donoghue, P. C. and M. A. Purnell. 1999. Mammal-like occlusion in conodonts. Paleobiology 25:58-
720 74.
721 Donoghue, P. C., M. A. Purnell, R. J. Aldridge, and S. Zhang. 2008. The interrelationships of 'complex'
722 conodonts (Vertebrata). Journal of Systematic Palaeontology 6:119-153.
723 Dray, S. and A.-B. Dufour. 2007. The ade4 package: implementing the duality diagram for ecologists.
724 Journal of Statistical Software 22:1-20.
725 Eroukhmanoff, F. 2009. Just how much is the G-matrix actually constraining adaptation? Evolutionary
726 Biology 36:323-326.
727 Eroukhmanoff, F. and E. I. Svensson. 2008. Phenotypic integration and conserved covariance
728 structure in calopterygid damselflies. Journal of Evolutionary Biology 21:514-526.
729 Escoufier, Y. 1973. Le traitement des variables vectorielles. Biometrics 29:751–760.
730 Gauchey, S., C. Girard, S. Adnet, and S. Renaud. 2014. Unsuspected functional disparity in Devonian
731 fishes revealed by tooth morphometrics? Naturwissenschaften 101:735-743.
732 Gingerich, P. D. 1983. Rates of evolution: effects of time and temporal scaling. Science 222:159-161.
733 Ginter, M., V. Hairapetian, and C. Klug. 2002. Famennian chondrichthyans from the shelves of North
734 Gondwana. Acta Geologica Polonica 52.
735 Girard, C., J.-J. Cornée, C. Corradini, A. Fravalo, and R. Feist. 2014. Palaeoenvironmental changes at
736 Col des Tribes (Montagne Noire, France), a reference section for the Famennian of north
737 Gondwana-related areas. Geological Magazine 151:864–884.
738 Girard, C., J.-J. Cornée, M. Joachimski, A.-L. Charruault, A.-B. Dufour, and S. Renaud. 2020.
739 Paleogeographic differences in temperature, water depth and conodont biofacies during the
740 Late Devonian. Palaeogeography, Palaeoclimatology, Palaeoecology 549:108852.
741 Girard, C. and S. Renaud. 2007. Quantitative conodont-based approaches for correlation of the Late
742 Devonian Kellwasser anoxic events. Palaeogeography, Palaeoclimatology, Palaeoecology
743 250:114-125.

744 Girard, C. and S. Renaud. 2008. Disentangling allometry and response to Kellwasser anoxic events in
745 the Late Devonian conodont genus *Ancyrodella*. Lethaia 41:383-394.
746 Girard, C. and S. Renaud. 2011. The species concept in a long-extinct fossil group, the conodonts.
747 Comptes Rendus Palevol 10:107-115.
748 Girard, C. and S. Renaud. 2012. Disparity changes in 370 Ma Devonian fossils: The signature of
749 ecological dynamics? PLoS ONE 7:e36230.
750 Girard, C., S. Renaud, and R. Feist. 2007. Morphometrics of the Late Devonian conodont genus
751 *Palmatolepis* : phylogenetic, geographical and ecological contributions of a generic approach.
752 . Journal of Micropalaeontology 26:61-72.
753 Girard, C., S. Renaud, and A. Sérayet. 2004. Morphological variation of *Palmatolepis* Devonian
754 conodonts: species versus genus. Comptes Rendus Palevol 3:1-8.
755 Guenser, P., L. Souquet, S. Dolédec, M. Mazza, M. Rigo, and N. Goudemand. 2019. Deciphering the
756 roles of environment and development in the evolution of a Late Triassic assemblage of
757 conodont elements. Paleobiology 45:440-457.
758 Guillaume, F. and M. C. Whitlock. 2007. Effects of migration on the genetic covariance matrix.
759 Evolution 61:2398-2409.
760 Hangartner, S., C. Lasne, C. M. Sgrò, T. Connallon, and K. Monro. 2019. Genetic covariances promote
761 climatic adaptation in Australian *Drosophila*. Evolution 74:326-337.
762 Helms, J. and W. Ziegler. 1981. Evolution oft he Pa elements in Palmatolepis Ulrich and Bassler,
763 1926. Pp. W98-99 *in* D. L. Clark, W. C. Sweet, S. M. Bergstrom, G. Klapper, A. R.L., F. H. T.
764 Rhodes, K. J. Muller, W. Ziegler, M. Lindstrom, J. F. Miller, and A. G. Harris, eds. Treatise on
765 invertebrate paleontology. Geological Society of America and University of Kansas Press,
766 Boulder, Lawrence.
767 Helms, J. J. 1963. Zur "Phylogenese" und Taxonomie von *Palmatolepis* (Conodontida, Oberdevon).
768 Geologie 4:449-485.
769 Hogancamp, N. J., J. E. Barrick, and R. E. Strauss. 2016. Geometric morphometric analysis and
770 taxonomic revision of the Gzhelian (Late Pennsylvanian) conodont *Idiognathodus simulator*
771 from North America. Acta Palaeontologica Polonica 61:477-502.
772 Hunt, G. 2004. Phenotypic variation in fossil samples: modeling the consequences of time-averaging.
773 Paleobiology 30:426-443.
774 Hunt, G. 2007. Evolutionary divergence in directions of high phenotypic variance in the ostracode
775 genus *Poseidonamicus*. Evolution 61:1560-1576.
776 Joachimski, M. M., S. Breisig, W. Buggisch, J. A. Talent, R. Mawson, M. Gereke, J. R. Morrow, J. Day,
777 and K. Weddige. 2009. Devonian climate and reef evolution: Insights from oxygen isotopes in
778 apatite. Earth and Planetary Science Letters 284:599-609.
779 Joachimski, M. M. and W. Buggisch. 2002. Conodont apatite d18O signatures indicate climatic cooling
780 as a trigger of the Late Devonian masse exctinction. Geology 30:711-714.
781 Jones, A. G., R. Bürger, S. J. Arnold, P. A. Hohenlohe, and J. G. Uyeda. 2012. The effects of stochastic
782 and episodic movement of the optimum on the evolution of the G-matrix and the response
783 of the trait mean to selection. Journal of Evolutionary Biology 25:2210-2231.
784 Jones, D., M. A. Purnell, and P. H. von Bitter. 2009. Morphological criteria for recognising homology in
785 isolated skeletal elements: comparison of traditional and morphometric approaches in
786 conodonts. Palaeontology 52:1243-1256.
787 Klapper, G. 1989. The Montagne Noire Frasnian (Upper Devonian) conodont succession. Pp. 449-468
788 *in* N. McMillan, A. Embry, and D. Glass, eds. Devonian of the World. Paleontology,
789 Paleoecology, Biostratigraphy. Canadian Society of Petroleum Geology, Calgary.
790 Klapper, G. and C. T. J. Foster. 1986. Quantification of outlines in Frasnian (Upper Devonian) platform
791 conodonts. Canadian Journal of Earth Sciences 23:1214-1222.
792 Klapper, G. and W. T. Kirchgasser. 2016. Frasnian Late Devonian conodont biostratigraphy in New
793 York: graphic correlation and taxonomy. Journal of Paleontology 90:525-554.
794 Langsrud, Ø. and B.-H. Mevik. 2012. ffmanova: fifty-fifty MANOVA., https://CRAN.R-
795 project.org/package=ffmanova.

796 Lazzari, V., C. Charles, P. Tafforeau, M. Vianey-Liaud, J.-P. Aguilar, J.-J. Jaeger, J. Michaux, and L.
797 Viriot. 2008. Mosaic convergence of rodent dentitions. Plos One 3:e3607.
798 Martínez-Pérez, C., E. J. Rayfield, H. Botella, and P. C. J. Donoghue. 2016. Translating taxonomy into
799 the evolution of conodont feeding ecology. Geology 44:247-250.
800 McGhee, G. R. J. 1996. The Late Devonian mass extinction — the Frasnian/Famennian crisis.
801 Columbia University Press, New York.
802 McGlothlin, J. W., M. E. Kobiela, H. V. Wright, D. L. Mahler, J. J. Kolbe, J. B. Losos, and E. D. Brodie III.
803 2018. Adaptive radiation along a deeply conserved genetic line of least resistance in *Anolis*
804 lizards. Evolution Letters 2-4:310-322.
805 McGuigan, K., S. F. Chenoweth, and M. W. Blows. 2005. Phenotypic divergence along lines of genetic
806 variance. The American Naturalist 165:32-43.
807 Mitteroecker, P. and F. Bookstein. 2009. The ontogenetic trajectory of the phenotypic covariance
808 matrix, with examples from craniofacial shape in rats and humans. Evolution 63:727-737.
809 Müller, K. J. 1956. Die Gattung *Palmatolepis*. Abhandlungen der senckenbergischen
810 naturforschenden Gesellschaft 494:1-70.
811 Nicoll, R. S. 1987. Form and function of the Pa element in the conodont animal. Pp. 77-90 *in* R. J.
812 Aldridge, ed. Paleobiology of conodonts. British micropaleontological Society Series, London.
813 Oksanen, J., F. G. Blanchet, M. Friendly, R. Kindt, P. Legendre, D. McGlinn, P. R. Minchin, R. B. O'Hara,
814 G. L. Simpson, P. Solymos, M. H. H. Stevens, E. Szoecs, and H. Wagner. 2017. vegan:
815 Community Ecology Package. R package version 2.4-3., https://CRAN.R-
816 project.org/package=vegan.
817 Pallares, L. F., B. Harr, L. M. Turner, and D. Tautz. 2014. Use of natural hybrid zone for genome-wide
818 association mapping of craniofacial traits in the house mouse. Molecular Ecology 23:5756-
819 5770.
820 Pallares, L. F., R. Ledevin, S. Pantalacci, L. M. Turner, E. Steingrimsson, and S. Renaud. 2017. Genomic
821 regions controlling shape variation in the first upper molar of the house mouse. eLife
822 6:e29510.
823 Peres-Neto, P. R. and D. A. Jackson. 2001. How well do multivariate data sets match? The advantages
824 of a Procrustean superimposition approach over the Mantel test. Oecologia 129:169-178.
825 Polly, P. D. 2004. On the simulation of the evolution of morphological shape: multivariate shape
826 under selection and drift. Palaeontologia Electronica 7:7A:28p.
827 Purnell, M. A. 1995. Microwear on conodont elements and macrophagy in the first vertebrates.
828 Nature 374.
829 Purnell, M. A. and P. C. J. Donoghue. 1997. Architecture and functional morphology of the skeletal
830 apparatus of ozarkodinid conodonts. Philosophical Transactions of the Royal Society, London
831 B 352:1545-1564.
832 Qannari, E. M., E. Vigneau, and P. Courcoux. 1998. Une nouvelle distances entre variables.
833 Application en classification. Revue de Statistique Appliquée 46:21-32.
834 R_Core_Team. 2017. R: A Language and Environment for Statistical Computing *in* R. F. f. S.
835 Computing, ed, Vienna, Austria.
836 Renaud, S. and J.-C. Auffray. 2013. The direction of main phenotypic variance as a channel to
837 morphological evolution: case studies in murine rodents. Hystrix, The Italian Journal of
838 Mammalogy 24:85-93.
839 Renaud, S., J.-C. Auffray, and J. Michaux. 2006. Conserved phenotypic variation patterns, evolution
840 along lines of least resistance, and departure due to selection in fossil rodents. Evolution
841 60:1701-1717.
842 Renaud, S., A.-B. Dufour, E. A. Hardouin, R. Ledevin, and J.-C. Auffray. 2015. Once upon multivariate
843 analyses: when they tell several stories about biological evolution. PLoS ONE 10:e0132801.
844 Renaud, S., B. Ecalle, P. Claisse, A.-L. Charruault, R. Ledevin, and C. Girard. 2021. Patterns of bilateral
845 asymmetry and allometry in Late Devonian Polygnathus conodonts. Palaeontology 64:137-
846 159.

Renaud, S. and C. Girard. 1999. Strategies of survival during extreme environmental perturbations: evolution of conodonts in response to the Kellwasser crisis (Upper Devonian). Palaeogeography, Palaeoclimatology, Palaeoecology 146:19-32.

Renaud, S., J. Michaux, J.-J. Jaeger, and J.-C. Auffray. 1996. Fourier analysis applied to *Stephanomys* (Rodentia, Muridae) molars: nonprogressive evolutionary pattern in a gradual lineage. Paleobiology 22:255-265.

Renaud, S., J. Michaux, D. N. Schmidt, J.-P. Aguilar, P. Mein, and J.-C. Auffray. 2005. Morphological evolution, ecological diversification and climate change in rodents. Proceedings of the Royal Society of London, Biological Sciences (serie B) 272:609-617.

Robert, P. and Y. Escoufier. 1976. A unifying tool for linear multivariate statistical methods: the RV-coefficient. Applied Statistics 25:257-265.

Roff, D. A. and T. Mousseau. 2005. The evolution of the phenotypic covariance matrix: evidence for selection and drift in *Melanoplus*. Journal of Evolutionary Biology 18:1104-1114.

Schluter, D. 1996. Adaptive radiation along genetic lines of least resistance. Evolution 50:1766-1774.

Scott, A. C. and C. Collinson. 1959. Intraspecific variability in conodonts: *Palmatolepis glabra* Ulrich & Bassler. Journal of Paleontology 33:550-565.

Spalletta, C., M. C. Perri, D. J. Over, and C. Corradini. 2017. Famennian (Upper Devonian) conodont zonation: revised global standard. Bulletin of Geosciences 92:1-27.

Steppan, S. J., P. C. Phillips, and D. Houle. 2002. Comparative quantitative genetics: evolution of the G matrix. Trends in Ecology and Evolution 17:320-327.

Thioulouse, J., S. Dray, A.-B. Dufour, A. Siberchicot, T. Jombart, and S. Pavoine. 2018. Multivariate Analysis of Ecological Data with ade4. Springer.

van den Boogaard, M. and B. Kuhry. 1979. Statistical reconstruction of the *Palmatolepis* apparatus (Late Devonian conodontophorids) at the generic, subgeneric, and specific level. Scripta Geologica 49:1-57.

Ziegler, W. and C. Sandberg. 1990. The Late Devonian standard conodont zonation. Courier Forschungsinstitut Senckenberg 121:1-115.

876 **Tables**

		MAN	RHO	PAN	PAN	DEF	DEF		Right
OTU	Age			*glabra*	*tenuipunctata*	*gracilis*	*minuta*	OTU	
DEF_63	363.45					86		DEF_63	43
DEF_62	363.80					58		DEF_62	36
DEF_61_1	364.60					62		DEF_61_1	40
DEF_59	366.00					69	2	DEF_59	33
DEF_56	366.21					45		DEF_56	24
PAN_56	366.21			40				PAN_56	21
PAN_51	367.10			102				PAN_51	102
PAN_50	367.22			72				PAN_50	37
DEF_42	368.31						71	DEF_42	40
RHO_42	368.31		61					RHO_42	27
DEF_41	368.48						34	DEF_41	20
RHO_41	368.48		49					RHO_41	25
RHO_39	368.60		149					RHO_39	80
PAN_37	369.22			12	30			PAN_37	21
PAN_35	369.77				65			PAN_35	31
MAN_23	371.47	51						MAN_23	27
MAN_22	371.70	95						MAN_22	68
MAN_12	372.12	56						MAN_12	28
MAN_11c	372.15	56						MAN_11c	37
MAN_08	372.34	39						MAN_08	16
MAN_07	372.38	83						MAN_07	49
MAN_06	372.43	48						MAN_06	24

877

878 **Table 1.** Sample size for each OTU. The label summarizes the subgenus (three-letters code) and the
879 stratigraphic level (from 06 to 63). An estimation of the absolute age is provided for each sample
880 according to the datation framework of Becker et al. (2020). MAN: *Manticolepis*. RHO: *rhomboidea*.
881 PAN: *Panderolepis*. DEF: *Deflectolepis*. For these two latter subgenera, the sample size is
882 decomposed into the two species present. Mixing only occurs in PAN_37 and DEF_59. Right: number
883 of right elements in the corresponding OTU.

884

ProcR \ P	Shape (bgPCA)	Pmax	P-RV	P-MB	Allometry
Shape (bgPCA)	-	0.0001	0.0001	0.0001	0.0002
Pmax	0.741	-	0.0001	0.0001	0.0001
P-RV	0.868	0.861	-	0.0001	0.0001
P-MB	0.817	0.655	0.840	-	0.0001
Allometry	0.592	0.632	0.700	0.707	-

Table 2. Relationships between the topologies between the 22 OTUs, based on the different descriptors of shape and shape variance. Protest results are shown (above the diagonal, P-values based on 10,000 permutations; below the diagonal, ProcR). P-RV: analysis of the P-matrices based on RV coefficients; P-MB: analysis of the P-matrices based on MB contrasts.

	pve	P	pve	P	pve	P
	Subgenus		Size (A0)		Asymmetry	
All	41.2%	< 2e-16	1.5%	< 2e-16	0.2%	1.02e-05
	Level		Size (A0)		Asymmetry	
Manticolepis	12.1%	< 2e-16	14.2%	< 2e-16	0.3%	0.0005
rhomboidea	6.8%	< 2e-16	13.1%	< 2e-16	0.4%	0.2070
Panderolepis	20.3%	< 2e-16	4.6%	< 2e-16	0.6%	0.0022
Deflectolepis	9.8%	< 2e-16	3.3%	< 2e-16	0.5%	0.0071

Table 3. Relative importance of the different sources of morphological variance: subgenus attribution in the total dataset and level within each subgenus; size (A0) and bilateral asymmetry (Right / Left Side). Percentage of variance explained (pve) are provided together with P-values estimated using the ffmanova procedure.

898 **Figures and Figure Captions**

899

900

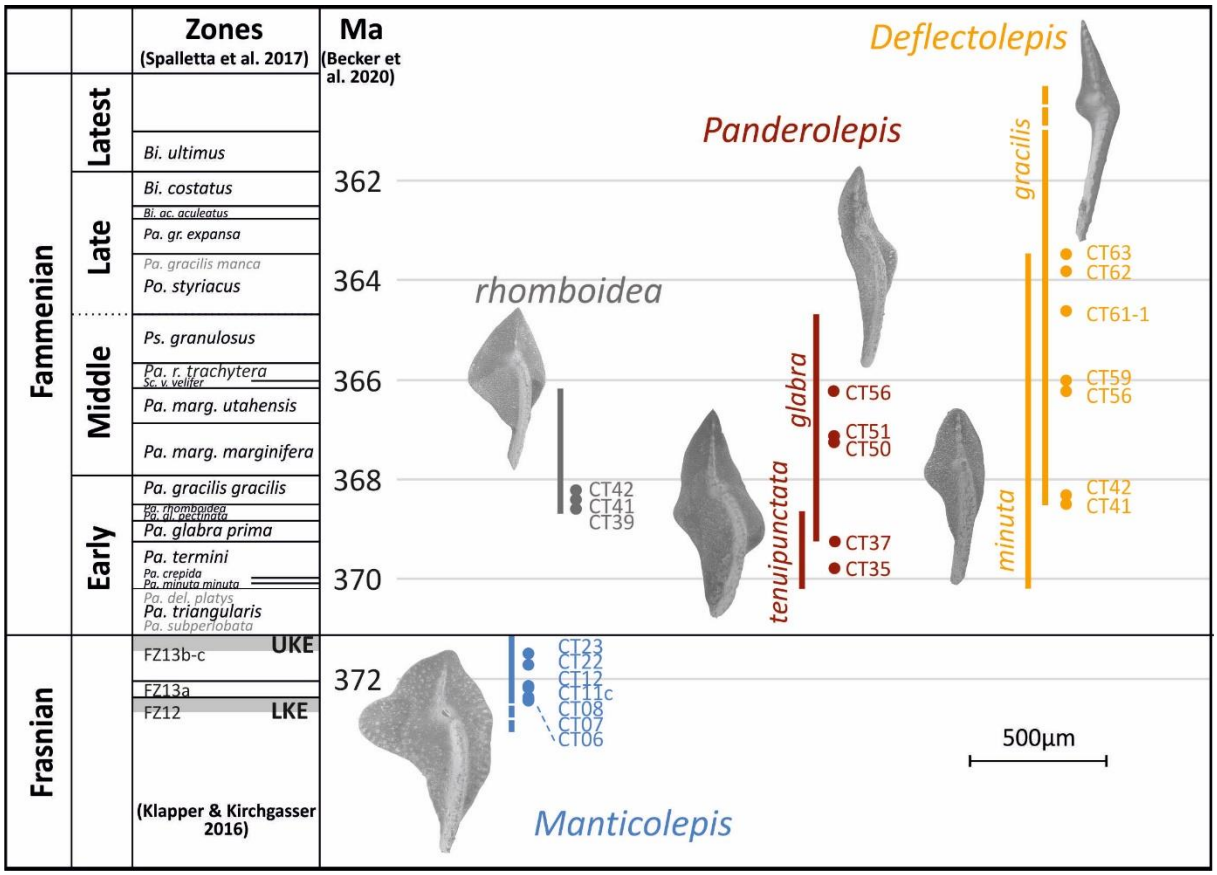

901

902

903 **Figure 1**. Illustration and temporal distribution of the studied subgenera of *Palmatolepis*. Code of the
904 levels: cf. Table 1 (e.g. CT42: level 42 of the Col des Tribes section). Stratigraphic zonation is provided
905 on the left (Frasnian: Klapper and Kirchgasser 2016; Famennian: Spalletta et al. 2017); absolute ages
906 after Becker et al. (2020). In grey, zones that have not been identified at the Col des Tribes section.
907 Illustrations are all to the same scale.
908 Labels of the illustrated specimens, from left to right: *Manticolepis* UM CTB 035 (CT22); *Palmatolepis*
909 *(Panderolepis) tenuipunctata* UM CTB 036 (mirror image; CT35); *Palmatolepis (Panderolepis) glabra*
910 UM CTB 037 (mirror image; CT48); *Palmatolepis rhomboidea* UM CTB 038 (mirror image; CT41);
911 *Palmatolepis (Deflectolepis) minuta* UM CTB 039 (CT37); *Palmatolepis (Deflectolepis) gracilis* UM CTB
912 040 (CT69).

913

914

915

916

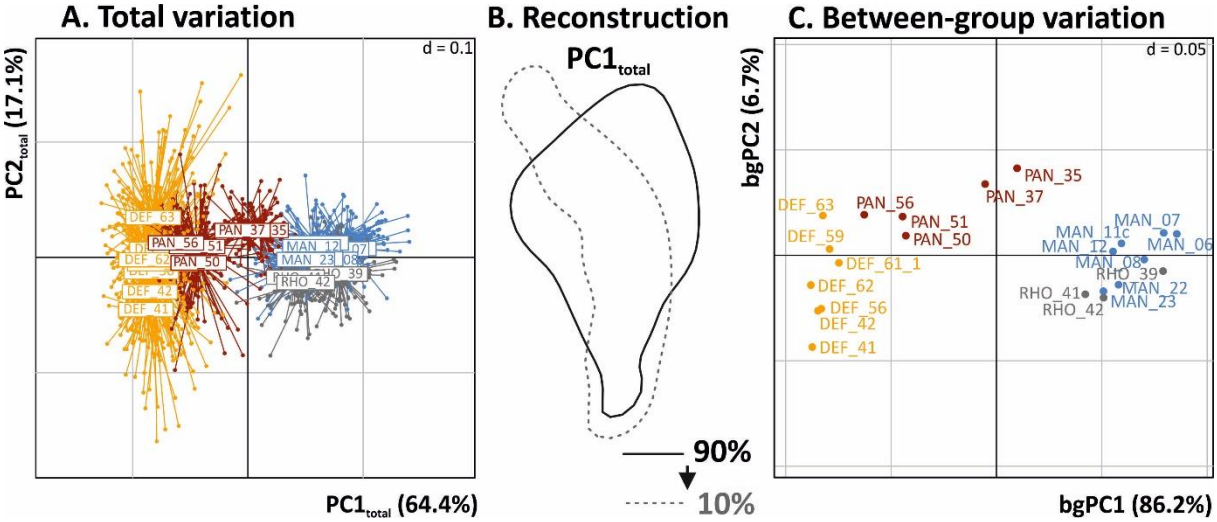

Figure 2. Shape differentiation between the 22 conodont Operational Taxonomic Units (OTU), based on the 18 shape variables describing the outline. A. Total variation, depicted on the first two axes of a PCA. Each dot represents one specimen. The color code corresponds to the four subgenera. B. Reconstructions of outlines illustrating the shape changes along the first PC axis. Grey dotted line: 10% smallest score along PC1. Full black line: 90% highest score along PC1. C. Between-group variation, depicted on the first two axes of a bgPCA. Each dot represents the mean of one conodont OTU. In A and C, the grid size is indicated by the d value at the upper right of the graph.

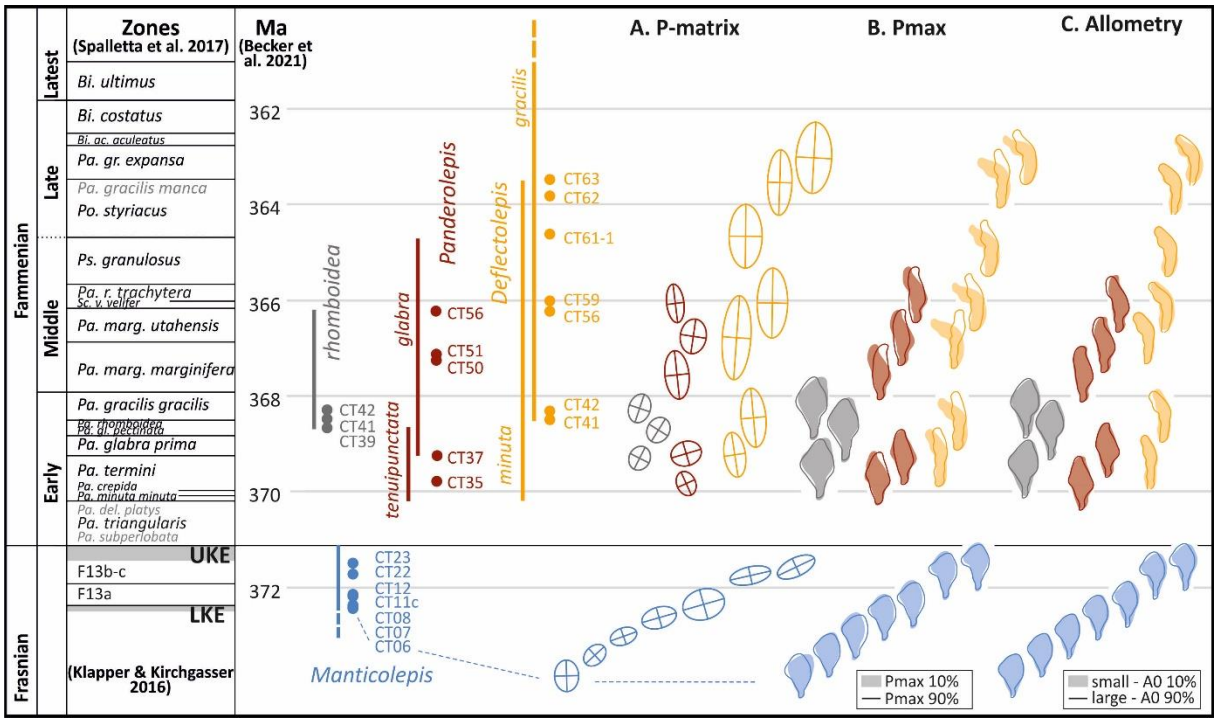

929

930 **Figure 3.** Visualization of the temporal variation of Pmax, P-matrices and allometry in the 22 OTUs.
931 (A) P-matrices, represented as ellipses defined by their first two axes, projected on the first principal
932 plane of PCA_{total} (see Fig. 2A). Their principal axis corresponds to the direction of the first eigenvector
933 (Pmax), the elongation represents the anisotropy of the variance (relative percentage of variance
934 represented by the first and second axes). (B) Pmax: the outlines in full lines and in transparency
935 visualize the shapes corresponding to 10% and 90% largest scores, respectively, on the first
936 eigenvector (Pmax). Since the +/- direction is arbitrary on such multivariate axes, the representation
937 has been homogenized: in transparent surfaces, outlines with a less developed platform and/or a
938 straighter shape. (C) Allometry: shapes corresponding to the 10% smallest size (in transparency) and
939 90% largest size (full line).

940

941

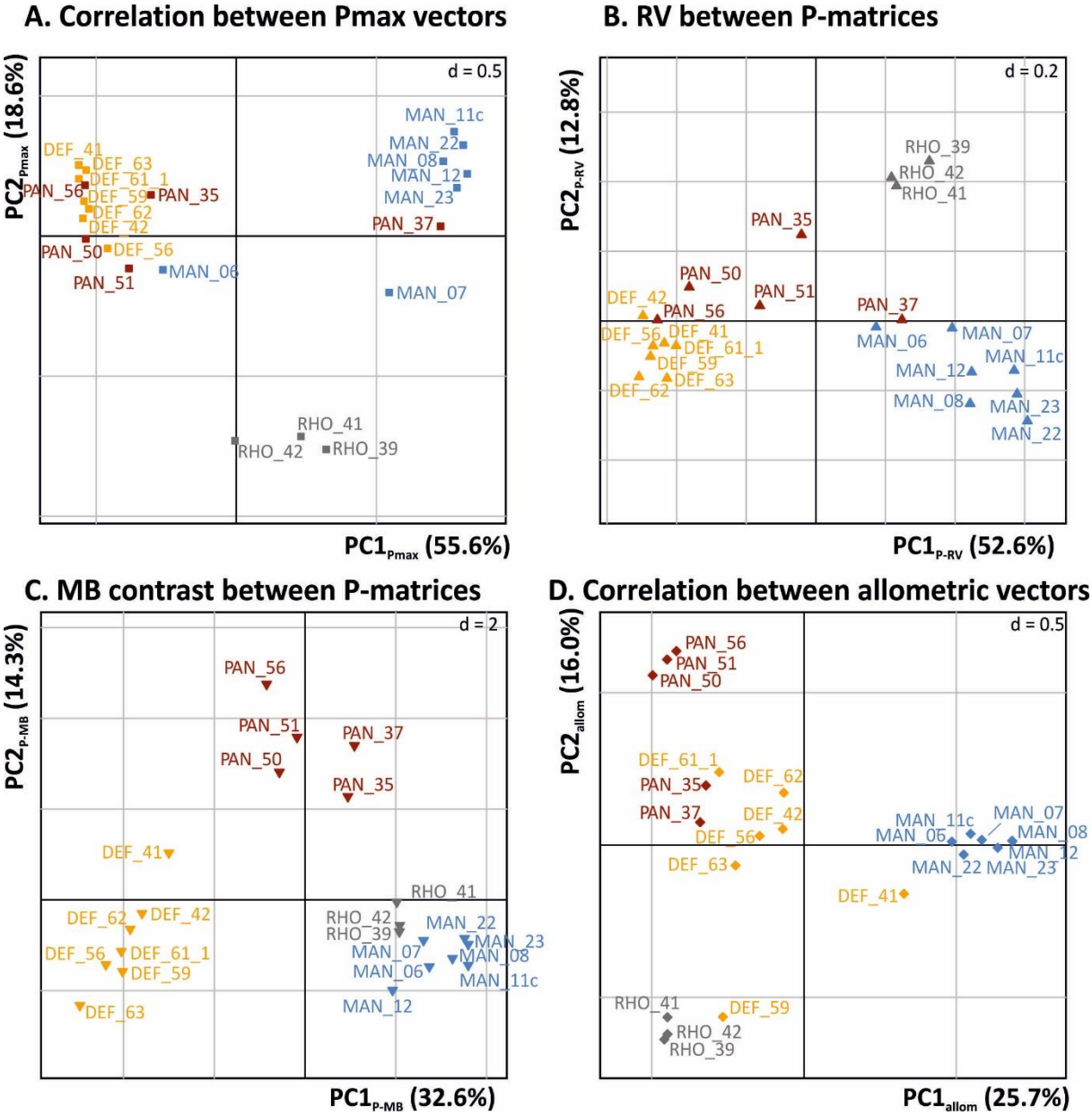

Figure 4. First two axes of PCOAs on four distance matrices describing the relationships between the 22 conodont OTUs. A. Distances derived from the correlation between Pmax vectors (squares). B. Distances based on the RV coefficients between P-matrices (up-pointing triangles). C. Contrast between P-matrices, based on the Mitteroecker & Bookstein ("MB") metric (down-pointing triangles). D. Distances based on the correlation between allometric vectors (diamonds).

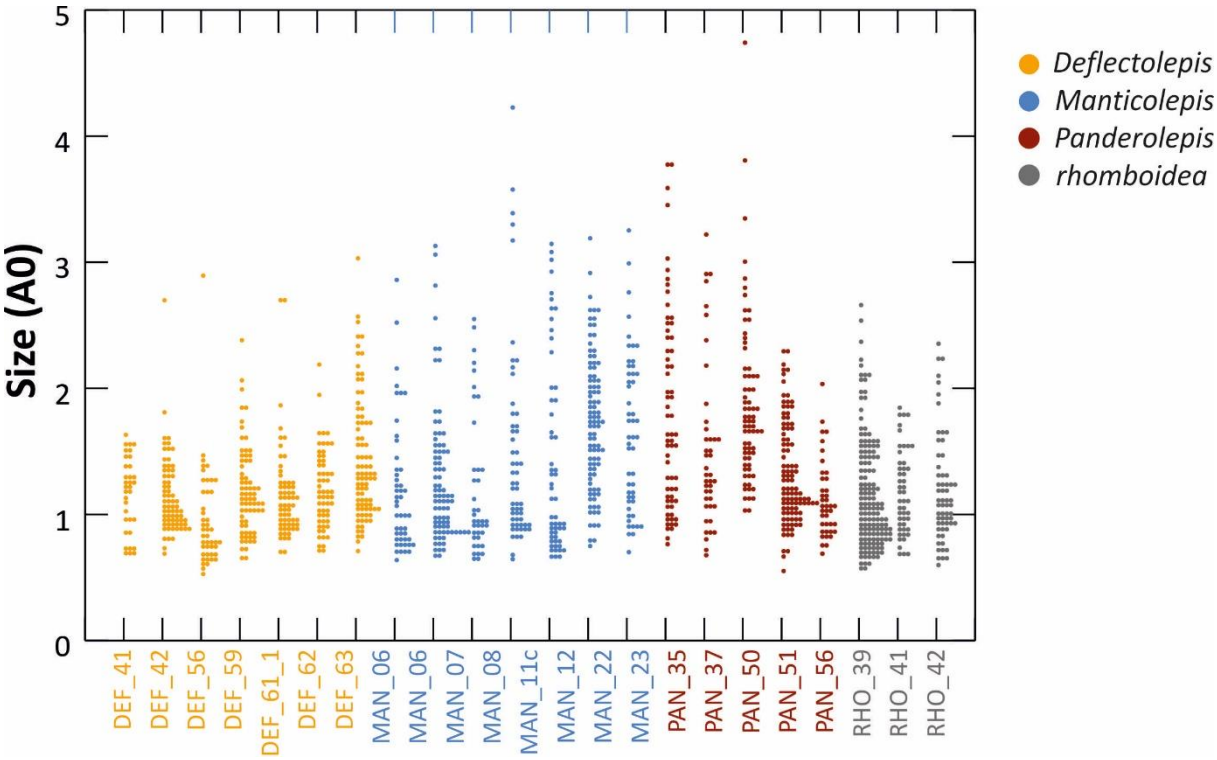

Figure 5. Size variation in the 22 conodont OTUs. Each dot corresponds to an element; size is estimated by the zero harmonic of the outline analysis.

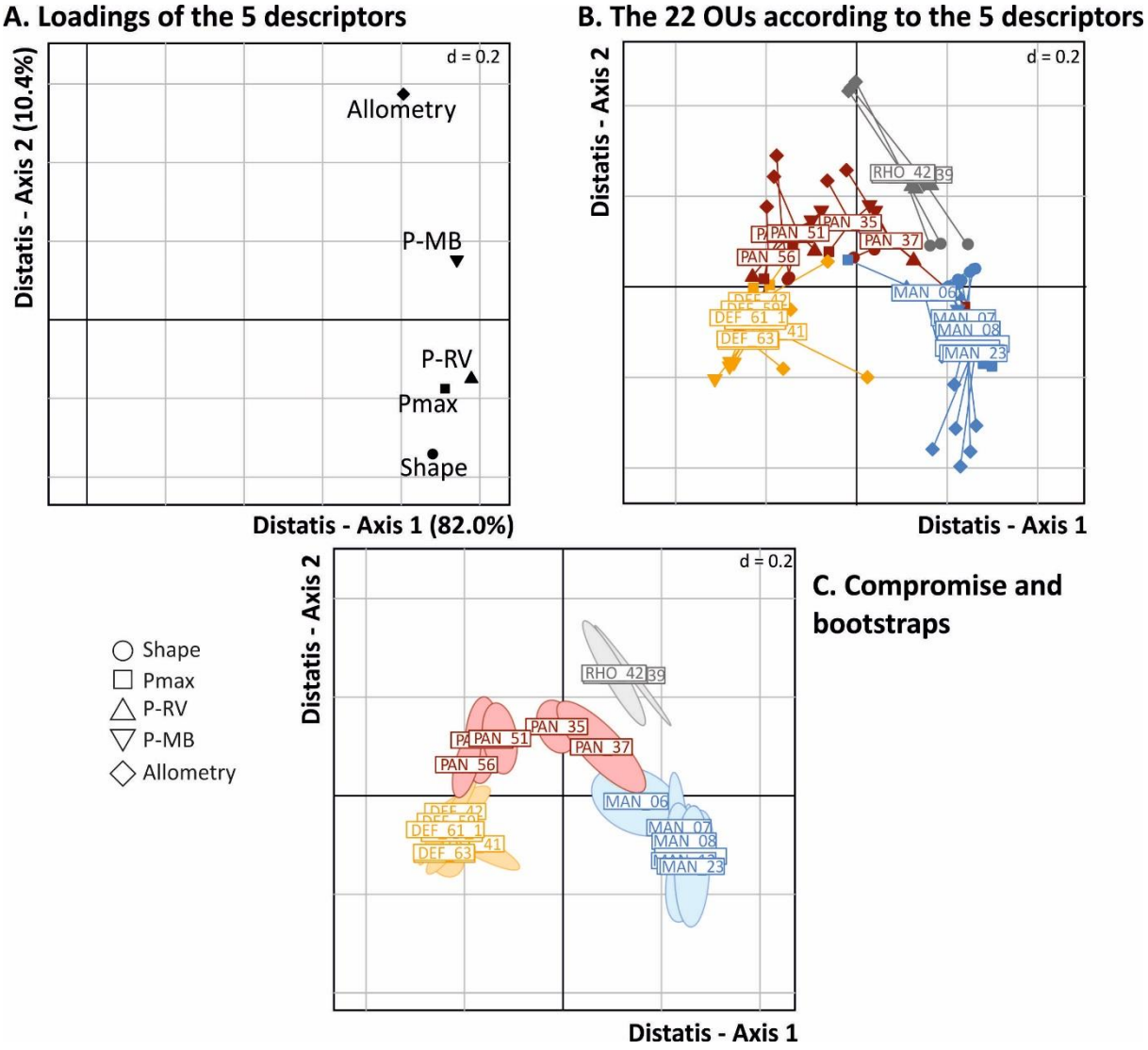

957

958 **Figure 6.** Simultaneous analysis of shape, Pmax, allometry, and P-matrices compared using RV ("P-
959 RV") and "MB" contrast ("P-MB") using the DISTATIS method. A. Relationship between the five
960 descriptors in the compromise space. B. Relationships between the 22 OTUs according to the five
961 descriptors in the compromise space. C. Position of the 22 conodont OTUs in the compromise space,
962 surrounded by bootstrap estimates.

963

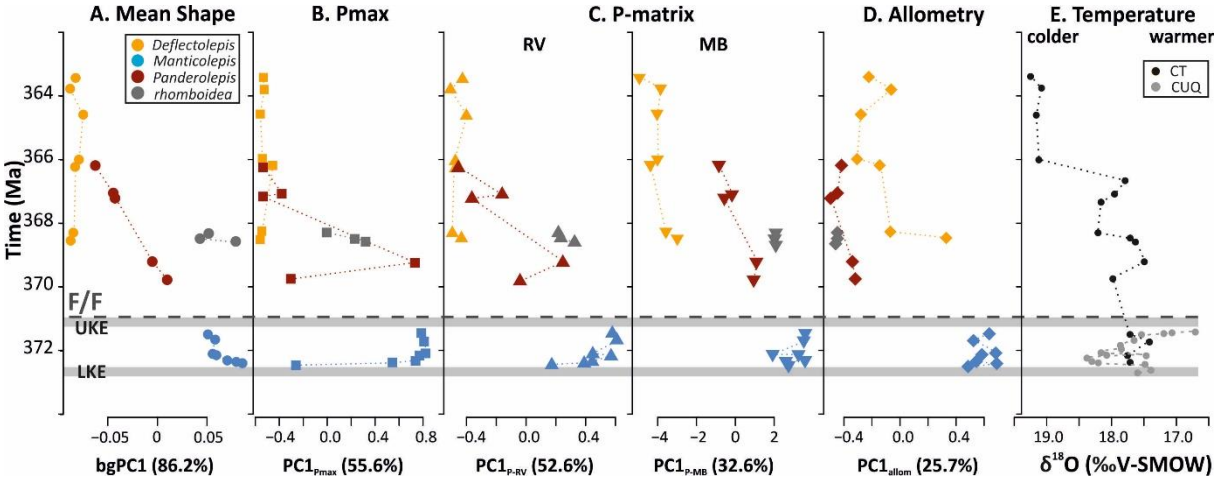

964

965

966 **Figure 7**. Temporal changes in mean shape, Pmax, P-matrix, and allometry compared with the
967 paleotemperature record. Variations in shape (A) is summarized by the scores of the 22 OTUs on
968 bgPC1; variations on Pmax (B), P-matrix (C) and allometry (D) are summarized by the scores on the
969 respective PC1. Paleotemperature (E) is estimated by $\delta^{18}O$ in the Col des Tribes (CT) levels considered
970 in this study (Girard et al. 2020). The Frasnian record is completed by data from the neighboring
971 Coumiac Upper Quarry (CUQ) section, in grey (Balter et al. 2008). These data have been corrected of
972 0.7‰ in order to account for different standards. Dotted line: Frasnian/Famennian boundary (F/F).

973

974

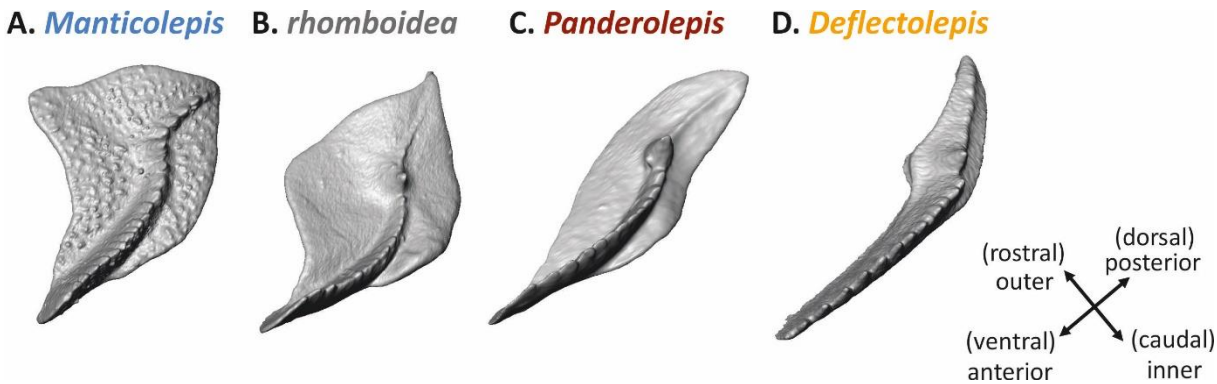

975

976

977 **Figure 8.** Tridimensional morphology of right P1 elements of the four subgenera considered:
978 *Manticolepis*, *rhomboidea*, *Panderolepis* and *Deflectolepis* (not to the same scale). (A) *Pa.*
979 *Manticolepis*, level CT22, length = 0.96 µm (UM CTB 078). (B) *Pa. rhomboidea*, level CT42, length =
980 0.96 µm (UM CTB 079); (C) *Pa.* (*Panderolepis*) *glabra*, level CT46, length = 0.47 µm (UM CTB 080); (D)
981 *Pa. (Deflectolepis) gracilis*, level CT63, length = 0.62 µm (UM CTB 081).